Environmental Pollution 220 (2017) 1112–1120

Contents lists available at ScienceDirect

Environmental Pollution

journal homepage: www.elsevier.com/locate/envpol

Microenvironmental air quality impact of a commercial-scale biomass heating system☆

Zheming Tong [a, 1], Bo Yang [a], Philip K. Hopke [b], K. Max Zhang [a, *]

[a] Sibley School of Mechanical and Aerospace Engineering, Cornell University, Ithaca, NY, 14853, United States
[b] Center for Air Resources Engineering and Science Clarkson University, NY, 13699, United States

ARTICLE INFO

Article history:
Received 14 July 2016
Received in revised form
7 November 2016
Accepted 8 November 2016
Available online 18 November 2016

Keywords:
Biomass emission
Near-source impact
Plume dispersion
LES
Emission control
Woodsmoke

ABSTRACT

Initiatives to displace petroleum and climate change mitigation have driven a recent increase in space heating with biomass combustion. However, there is ample evidence that biomass combustion emits significant quantities of health damaging pollutants. We investigated the near-source micro-environmental air quality impact of a biomass-fueled combined heat and power system equipped with an electrostatic precipitator (ESP) in Syracuse, NY. Two rooftop sampling stations with $PM_{2.5}$ and CO_2 analyzers were established in such that one could capture the plume while the other one served as the background for comparison depending on the wind direction. Four sonic anemometers were deployed around the stack to quantify spatially and temporally resolved local wind patterns. Fuel-based emission factors were derived based on near-source measurement. The Comprehensive Turbulent Aerosol Dynamics and Gas Chemistry (CTAG) model was then applied to simulate the spatial variations of primary $PM_{2.5}$ without ESP. Our analysis shows that the absence of ESP could lead to an almost 7 times increase in near-source primary $PM_{2.5}$ concentrations with a maximum concentration above 100 μg m^{-3} at the building rooftop. The above-ground "hotspots" would pose potential health risks to building occupants since particles could penetrate indoors via infiltration, natural ventilation, and fresh air intakes on the rooftop of multiple buildings. Our results demonstrated the importance of emission control for biomass combustion systems in urban area, and the need to take above-ground pollutant "hotspots" into account when permitting distributed generation. The effects of ambient wind speed and stack temperature, the suitability of airport meteorological data on micro-environmental air quality were explored, and the implications on mitigating near-source air pollution were discussed.

1. Introduction

Recently, initiatives to displace petroleum and climate change mitigation have driven an increase in space heating with biomass combustion in the world (Demirbas, 2005). However, biomass (dominated by wood) combustion is a source of primary $PM_{2.5}$ emission, and can be a significant contributor to ambient wintertime $PM_{2.5}$ concentrations (Boman et al., 2003; Larson and Koenig, 1994; Maykut et al., 2003; Naeher et al., 2007; Schauer et al., 1996; Wang et al., 2011a; Zheng et al., 2002). Glasius et al. (2006) measured the contribution from residential wood combustion to local particulate matter (PM) concentrations and found it to be comparable to a busy roadway in Denmark. A similar finding was reported by Ries et al. (2009), which estimated the winter season intake fraction based on spatial temporal statistical models in Vancouver, Canada. Boman et al. (2003) and Naeher et al. (2007) reviewed studies on the health effect of ambient air pollution in relation to residential wood combustion, indicating that biomass burning is not less toxic than other emission sources of PM.

A critical aspect of assessing health risks from wood smoke exposure is the spatial variation of PM. The location of the emission sources, the surrounding urban landscape, and micro-meteorology all influence the spatial pattern of PM and unfavorable conditions could create "hotspots" of elevated concentrations. To date, only a few studies have focused on the spatial variation of wood-burning PM, and those studies mostly focused residential-scale wood combustion. For example, Larson et al. (2007) and Su et al. (2008, 2015) developed land use regression (LUR) models to predict the

☆ This paper has been recommended for acceptance by Eddy Y. Zeng.
* Corresponding author.
E-mail address: kz33@cornell.edu (K.M. Zhang).
[1] Now at the Center for Green Buildings and Cities, Graduate School of Design, Harvard University, Cambridge, MA, 02138.

http://dx.doi.org/10.1016/j.envpol.2016.11.025

spatial variation of woodsmoke levels for urban areas. Allen et al. (2011) combined mobile and fixed-location monitoring to develop a LUR model for predicting the spatial variation of $PM_{2.5}$ in an rural area of upstate New York with valley topography.

Commercial-scale biomass-based heating systems are often located in populous urban areas with relatively short stack height, and few studies have investigated their impacts. Petrov et al. (2015) evaluated the health risk associated with a biomass combined heat and power (CHP) facility at a university campus using a dispersion model (CALPUFF) and the intake fraction method. For sites surrounded by major urban structures such as street canyons, neither LUR models nor dispersion models are able to fully take into account the complex turbulent flow field that significantly alters the plume trajectory (Pullen et al., 2005). By contrast, Computational Fluid Dynamics (CFD) is more capable of capturing the near-source flow patterns and plume dispersion but at greater computing cost (Gousseau et al., 2011; Tominaga and Stathopoulos, 2011; Tong et al., 2012; Wang et al., 2011b; Steffens et al., 2013).

The primary objective of this study is to evaluate the near-source micro-environmental impact of a commercial-scale biomass boiler with and without emission control using both on-site measurement and dispersion simulations using the CFD-based CTAG model. The selected biomass stack in this study was uniquely located adjacent to two large buildings with rooftop access, which allowed the measurement of the biomass plumes under varying wind directions. A fuel-based emission rate was derived from near-source measurement with emission control. The performance of CTAG simulations was evaluated with on-site wind and $PM_{2.5}$ measurements, and then we applied CTAG to simulate scenarios without emission control. In the second part of the study, we explored various design parameters including stack temperature and ambient weather conditions to provide recommendations for siting biomass-fueled heating equipment in order to mitigate near-source air pollution.

2. Experimental method

2.1. Site description

The Combined Heat and Power (CHP) facility with a wood pellet-fired boiler and an electrostatic precipitator (ESP) is located in the Gateway Building on the campus of SUNY College of Environmental Science and Forestry (ESF) in Syracuse, NY. The biomass CHP system was designed to supply both thermal and electrical energy for five campus buildings. ESP is generally accepted as a reliable and efficient particulate control device with low operating and maintenance costs (Lind et al., 2003). However, currently it is still rare for distributed biomass energy systems to be equipped with ESPs. During the field measurements, the system did not generate electricity, serving as a boiler for heating purpose only.

Even though the Gateway Building is located in an academic setting, the nearby structures including the Carrier Dome (CD) and Illick Hall (IH) make the surrounding area a good representation of a complex urban built environment (Fig. 1). The exhaust stack is on the roof of the Gateway Building about 16 m above the ground level, surrounded by CD (~42 m) and IH (~26 m). The presence of these two tall buildings with accessible rooftop areas allowed us to set up measurement stations and capture the near-source stack plumes. Other buildings are located further from the stack with lower heights as shown in Fig. 1.

2.2. Instrumentation

Two personal DataRam (pDR-1200, Thermo Scientific, Boston, MA, USA) with $PM_{2.5}$ size-selective cyclones were deployed to continuously collect data every 6 s. One CO_2 sensor (MI70, VAISALA) and one CO sensor (IAQ-CALC, TSI Model 7545) were employed in combination with $PM_{2.5}$ measurements to detect concurrent concentration spikes at the IH station. Three 3-D Gill sonic anemometers were strategically deployed to measure the instantaneous wind speed and direction at 1 Hz. Before the field trip, the two pDRs were cross-calibrated by co-locating them next to a traffic source to rectify any systematic differences between them. Three anemometers were cross-calibrated in an environmental wind tunnel to ensure consistency among them. Calibration details are available in the Supporting Information as shown in Figs. S1 and S2.

2.3. Sampling locations

Two rooftop sampling stations (CD and IH station) were established such that one can capture the plume while the other one serves as the background in comparison depending on the wind direction (Fig. 1). At the CD station, the pDR was placed on south edge facing the stack. At the IH station, the pDR and CO/CO_2 sensors were placed near the west edge of the roof facing the stack (Fig. 1). All instruments were raised vertically away from the floor in order to avoid boundary layer effect. The arrangement of the three anemometers was made according to the prevailing wind direction (West). One station was installed upwind of the Gateway Building 4.3 m from the ground level. The second anemometer station was installed at the green roof level of the Gateway Building 2.5 m from the floor. The third station was placed outside the south exit of the Gateway Building 2.6 m from the floor. The field measurements took place from March 16 to 20, 2015, respectively. A preliminary field campaign was conducted a month earlier (from February 16 to 19, 2015). There was a heavy snowstorm during the field campaign in which the rooftop access was not available due to safety reasons. The data presented in Section 4 corresponds to non-snow periods that did not exceed recommended operating temperature and humidity by the manufacturer (−10°–50 °C and 10–95% RH) during the campaign.

3. Model description

To evaluate the near-source air quality impacts of a biomass system in an urban neighborhood, it is essential to accurately model plume dispersion where exhaust momentum/buoyancy, surrounding structures and micrometeorology play significant roles. Based on CFD, the Comprehensive Turbulent Aerosol Dynamics and Gas Chemistry (CTAG) model was designed to resolve turbulent reacting flows, aerosol dynamics, and gas chemistry in complex urban environments. A full description of the model's theoretical background and implementation was presented in our previous work (Wang and Zhang, 2012; Wang et al., 2013a; Wang et al., 2013b; Steffens et al., 2014; Tong et al., 2016). In particular, a similar methodology was applied to simulate plume dispersion of diesel backup generators in New York City (Tong and Zhang, 2015). Large Eddy Simulation (LES) was employed to resolve the unsteady turbulent flow field. A dynamic subgrid model for LES was chosen, which allows the Smagorinsky constant to vary in space and time (Germano et al., 1991). A logarithmic wall function was applied to the near-wall region since it was computationally impractical to resolve every viscous sublayer in a large domain (Launder and Spalding, 1974). LES is a suitable turbulence model for simulating unsteady flow over bluff bodies like urban canopies, because it explicitly resolves large scale eddies created by urban structures, and only require models the small-scale, unresolvable turbulent motion which is less influenced by the physical boundaries (Rodi, 1997; Xie and Castro, 2006).

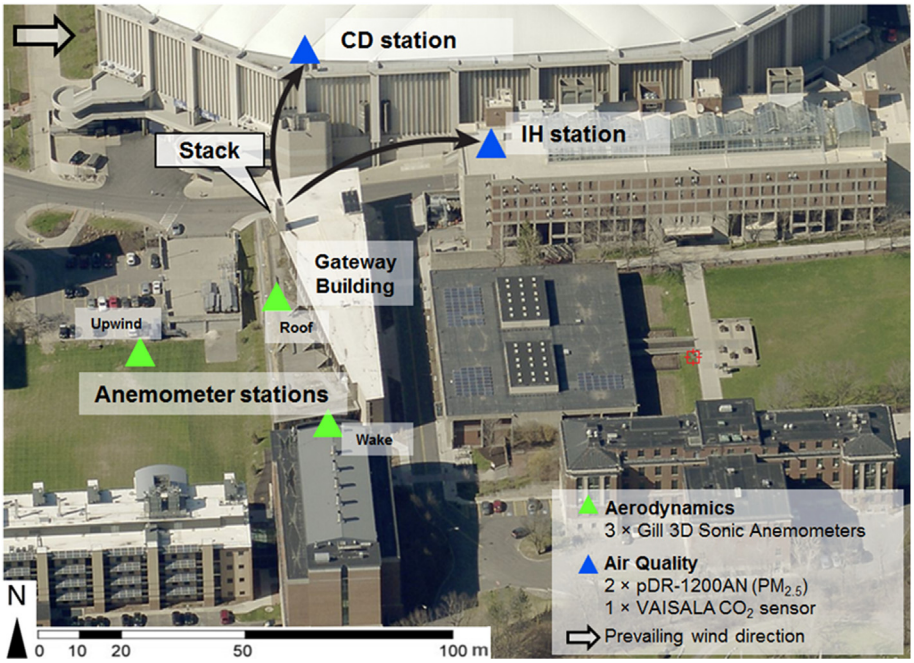

Fig. 1. Satellite image of the studied site overlaid with wind and air quality sampling points (CD: Carrier Dome; IH: Illick Hall).

Several LES studies were conducted to model plume dispersion with realistic urban geometries. The study presented here generally followed the guidelines developed from them (Gousseau et al., 2011; Salim et al., 2011; Tominaga and Stathopoulos, 2011; Tseng et al., 2006). In addition, we considered site-specific meteorological parameters such as friction velocity, atmospheric stability length, and sensible heat flux to construct the inlet profiles, which is critical to near-surface plume dispersion (Sini et al., 1996; Wood and Jarvl, 2012).

3.1. Boundary conditions

The size of the computational domain was roughly 473 m × 372 m × 168 m (Fig. 2), meshed with 12 million unstructured elements with prism layers near the wall. The size of the grid cells ranged from a few centimeters at the stack to a few meters near the boundaries of the domain. Although grid-independent solution is not available for LES (Klein, 2005), sensitivity analysis was conducted to ensure that the time-averaged results of the selected grid did not vary notably with finer resolution, as elaborated in Section S6 in the Supporting Information. Boundary conditions such as vertical wind and temperature profiles are critical inputs to neighborhood scale simulations. In this study, on-site wind measurement data were used to generate those profiles rather than using data from the nearest airport, which was a common approach during permitting process. Following the methods described in Tong and Zhang (20105), we employed a semi-empirical method to create site-specific inflow considering atmospheric stability, which plays a critical role in plume dispersion. Stability parameter (i.e., Monin-Obukhov length L) was computed from a meteorological processor, AERMET, developed by U.S. EPA (Cimorelli et al., 2005; USEPA, 2004). Friction velocity (u^*) was then computed based on measured wind speed upwind to the gateway building and Monin-Obukhov length from AERMET. The

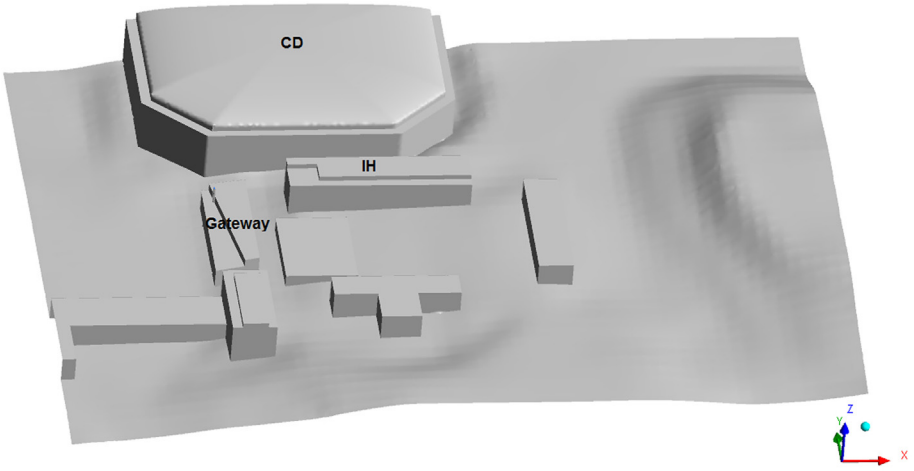

Fig. 2. Modeling domain for CTAG simulation.

time-dependent feature of the inlet turbulence profile was simulated by the vortex method, where random vortices at the inlet flow plane for the wall-normal components were generated, providing a spatial correlation (Kraichnan, 1970; Mathey et al., 2006). The standard wall function with a roughness modification was employed (Cebeci and Bradshaw, 1977; Launder and Spalding, 1974). The sand-grain roughness height k_s and roughness constant C_S in the wall function were estimated from the aerodynamic roughness height z_0 based on the relationship derived by Blocken (2015). Symmetry boundary condition is applied on the top of the domain as slip walls with zero-shear. At the flow outlet (vary with wind direction), zero diffusion flux of all flow variables was specified. In the model, we treated primary $PM_{2.5}$ as a tracer species, i.e., assuming that gas/particle partitioning near stacks would not significant change the primary $PM_{2.5}$ mass near the sources. Aerosol dynamics changes the particle size distribution in the near-source environment but have less effect on the primary $PM_{2.5}$ mass concentration. In this study, we only considered particle deposition on walls. This assumption is subject to future investigation. The biomass boiler was treated as the only source with background $PM_{2.5}$ determined from the measurement.

3.2. Stack parameters

The biomass CHP was installed in the basement of the Gateway Building. A list of stack parameters is shown in Table 1. The exhaust temperature and fuel consumption rate were obtained from on-site measurement. The fuel consumption rate was computed based on auger revolution with 2.45 kg of pellets fed into the boiler per revolution. The fuel-based primary $PM_{2.5}$ emission factor was derived based on near-source measurement (to be described in Section 3.2). In practice, proper sizing, system optimization, design, and measurement and verification are all critical to commercial solid-fueled biomass boiler systems, all of which greatly influence the emission factor of the boiler. The ESP collection efficiency was obtained from the onsite stack test performed by Wang et al. (2015), which was also consistent with the value listed in the permit application (RSG Inc, 2011).

3.3. Fuel-based emission factor

The fuel-based emission factor, defined as the mass of pollutant emitted per mass of fuel consumed (g kg^{-1}), was derived based on near-source measurement and the carbon balance method, relating the emission of carbon-containing species in exhaust to fuel consumption (Stedman, 1989; Wang et al., 2012). We consider CO_2 and CO as they account for a majority of the carbonaceous products during the combustion process (Wang et al., 2009; Westerdahl et al., 2009). The emission factor was calculated as follows:

$$EF_P = \frac{\Delta[PM_{2.5}]}{\Delta[CO_2] \times \frac{MW_C}{MW_{CO_2}} + \Delta[CO] \times \frac{MW_C}{MW_{CO}}} \times w_c \quad (1)$$

where $\Delta[PM_{2.5}]$, $\Delta[CO_2]$, and $\Delta[CO]$ represent the increase of $PM_{2.5}$, CO_2 and CO over the background, respectively. w_c is the mass fraction of carbon in the wood pellet, which was chosen to be 46.8% according to the pellet analysis by Chandrasekaran et al. (2011). MW is molecular weight. EF_P is converted to emission rate [kg s^{-1}] by multiplying the fuel consumption rate Q [kg s^{-1}].

3.4. Uncertainties

In general, micro-environmental air quality modeling involves many uncertainties. Studies in the past have shown that the uncertainties in ground-level concentration prediction could lead to mean biases of ±20–40% (Hanna, 1993). The uncertainties associated with the field measurement and CTAG model were discussed here. For the experimental component, the main uncertainty is attributed to sampling error, which can be split into fixed and random error (Moffat, 1988). The fixed error is associated with the instrument (e.g. accuracy, resolution), and the random error arises from many sources, e.g. background noise. The accuracy and resolution of the instruments employed in the field is presented in Table S1 (Supporting Information). The random error was computed with the bootstrap algorithm, which is a method to directly estimate the probability density function of calculated data from the measurement. We computed the 95% confidence intervals of the mean $PM_{2.5}$ concentration, wind speeds, and wind directions. Then, we estimated the total experimental error using the root sum square technique shown in Equation (2). The error bars of the total experimental error are displayed in Figs. 3 and 4.

$$\delta_{total} = \sqrt{\delta_{fixed}^2 + \delta_{random}^2} \quad (2)$$

In contrast with the experimental component, the uncertainty associated with CTAG model could arise from both model physics and model inputs. The simplification of onsite building geometry and turbulence modeling contributed to the uncertainties in model physics. On the other hand, the fuel-based emission factor and meteorology-based boundary conditions were major sources of uncertainty for model inputs. Here we only presented the uncertainty associated with the fuel-based emission factor based on the experimental error of air quality measurement (Fig. 5). The uncertainty in relation to model physics is a complex topic and subject to future study.

Table 1
Stack parameters.

Parameter	Value	Reference
Exhaust Flow Rate [m^3/s]	1.8	Permit Application
Exhaust Temperature [K]	350	On-site Measurement
Stack Diameter [m]	0.4	Permit Application
Stack Height[a] [m]	16.7	Permit Application
$PM_{2.5}$ Emission Factor [g kWh^{-1}]	0.29 (0.25–0.34)[b]	Section 3.3
$PM_{2.5}$ Emission Rate [g s^{-1}]	0.23	Section 3.3
Fuel Consumption Rate Q [kg/s]	0.15	On-site Measurement
ESP Collection Efficiencyη	85%	On-site Measurement[c]

[a] Stack height is measured from the ground level of the building.
[b] The error range of the fuel-based emission factor is determined from bootstrap analysis on the measurement data.
[c] The stack test was performed by Wang et al. (2015) on site.

4. Results and discussion

4.1. Model evaluation

The data from March 19, 2015 were selected for simulation as there was a noticeable shift in wind direction (from South to West) while the load of biomass boiler remained steady. Both IH and CD stations detected plume signals at different times, and we employed the fuel-based emission factor derived from the measurement on the IH station to predict the concentration at the rooftop of the CD station. Three concurrent biomass plume spikes were identified with high confidence on the IH station characterized by the synchronized CO_2 and $PM_{2.5}$ concentrations (Fig. S3 a-c of the Supporting Information). Another three spikes were observed at the CD station (Fig. S3 d-f of the Supporting Information). Fig. 3 illustrated a comparison between simulated and

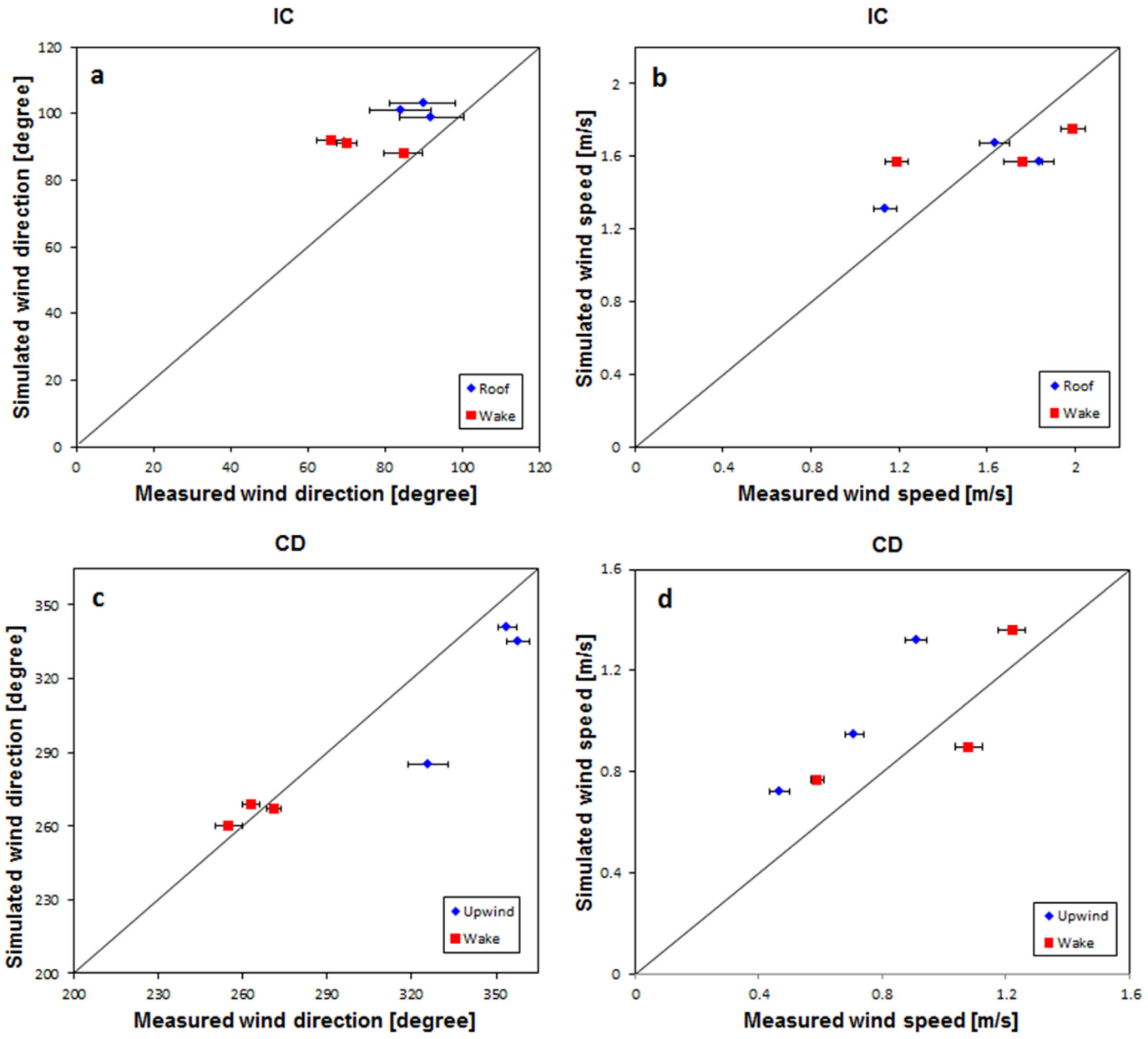

Fig. 3. Comparisons between simulated and measured wind speed and direction; a and b are under the boundary condition where wind is from the west to Illick Hall (IH). c and d are under the boundary condition where the wind is from the south to the Carrier Dome (CD). "Roof", "Wake" and "Upwind" indicate the locations of each anemometer station as displayed in Fig. 1. Error bars represent the total measurement error.

measured wind speed and directions. In general, it showed a good agreement between predicted and on-site measurement for flow fields, indicating the model's capability of capturing the flow fields under the influence of nearby buildings. The comparison between simulated and measured $PM_{2.5}$ concentrations were depicted in Fig. 4, and an adequate agreement was shown. The predictions at the IH station agreed better than that at the CD station, as the emission rate was derived based the measurement on the IH station. The discrepancies in both wind speed/direction and $PM_{2.5}$ concentrations were likely due to simplified building geometry and uncertainties in the fuel-based emission factor.

4.2. With and without emission control

The emission factor in the absence of the ESP was derived based on the collection efficiency according to the on-site testing (Table 1). Contour plots of $PM_{2.5}$ concentrations in the surrounding environment with and without ESP were displayed in Fig. 5. In the absence of ESP control, our analysis showed a significant increase in near-source primary $PM_{2.5}$. The maximum ground-level concentration without ESP occurred in the wake zone behind IH exceeding 35 $\mu g\ m^{-3}$, which was nearly seven times greater than that with ESP. In addition, the primary $PM_{2.5}$ concentrations on the rooftop of the adjacent building (Illick Hall) could reach over 100 $\mu g\ m^{-3}$ without ESP, and the implications were discussed in Section 4.3.

4.3. Ground-level vs. above-ground concentrations

Our previous study discussed how the ground-level concentration and plume trajectories vary with different street canyon configurations (Tong and Zhang, 2015). Fig. 6 presented a comparison between ground-level primary $PM_{2.5}$ concentrations and

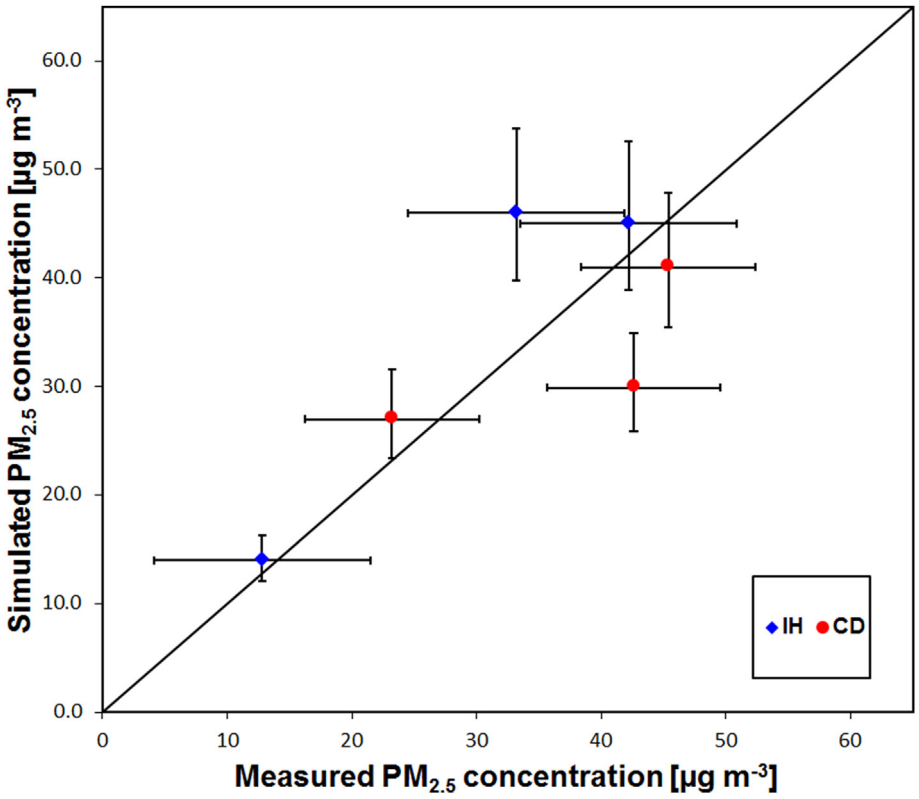

Fig. 4. Comparison between simulated and measured $PM_{2.5}$ concentrations in plumes. Error bars for total measurement errors are applied on the measurement data. Error bars of the simulation data are generated based on the uncertainty in the fuel-based emission factor.

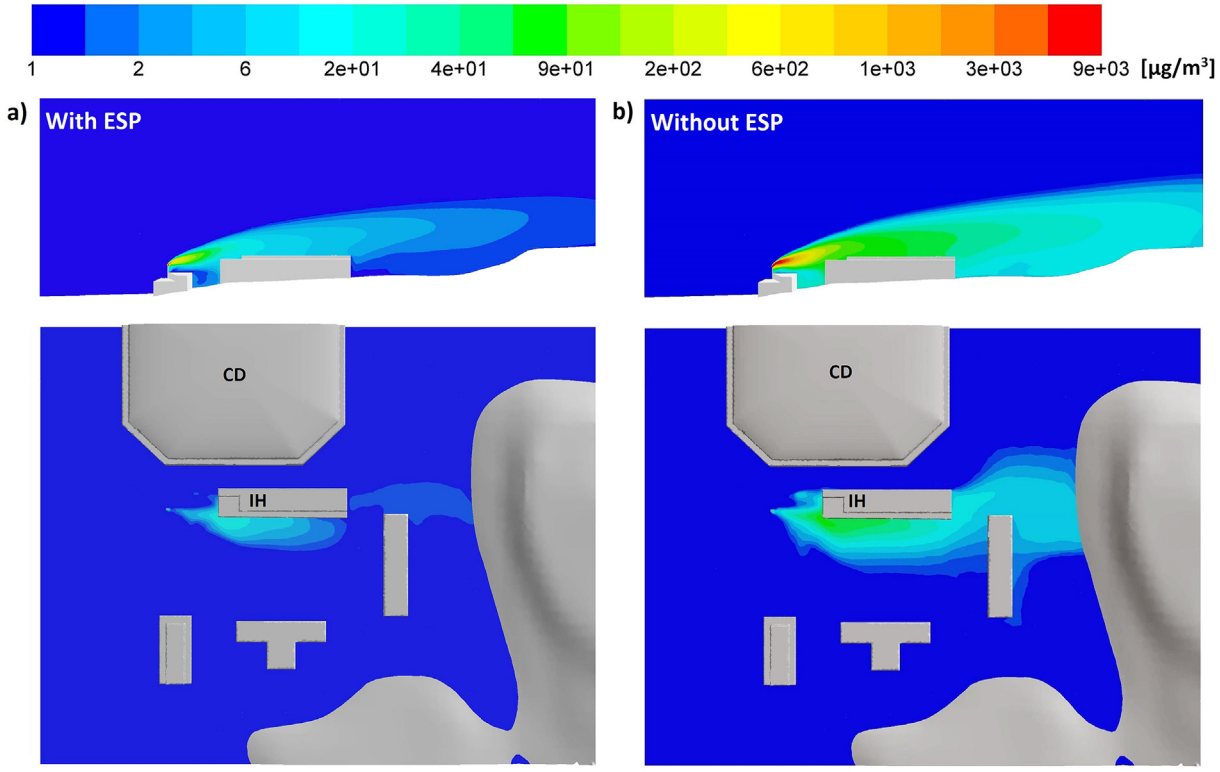

Fig. 5. a) Primary $PM_{2.5}$ concentration [μg m^{-3}] contour plot (top and side view) with ESP; b) Primary $PM_{2.5}$ concentration [μg m^{-3}] contour plot without ESP (top and side view). The reference plane of the top view is taken at 1.5 m above the ground outside IH. Its location is displayed in Fig. S4 of the Supporting Information.

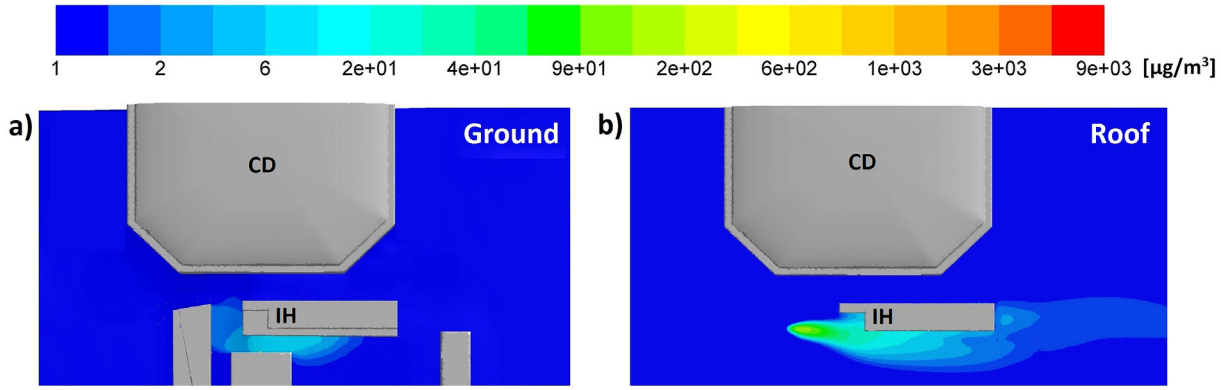

Fig. 6. a) Contour plot of primary $PM_{2.5}$ concentrations at near-ground level with ESP [μg m^{-3}]; b) Contour plot of primary $PM_{2.5}$ concentrations at roof level with ESP.

the concentration at rooftop level of IH (with ESP). The maximum concentration could exceed 35 μg m^{-3} at the rooftop and windward façade, even though the concentration at the ground level was nearly zero (Fig. 6). However, most permitting processes of new power plants in the U.S only consider ground-level concentrations, which could underestimate the health risk from above-ground pollutant "hotspots". These spots pose potential health risks to building occupants since particles can readily penetrate through infiltration, natural ventilation, and fresh air intakes on the rooftop (Petersen et al., 2002).

4.4. Ambient wind speed

The influences of several physical parameters including stack temperature, ambient wind, and the selection of weather data source on plume dispersion were explored in the following sections. Here we conducted a sensitivity study on the incoming wind speed by increasing the baseline wind speed to two and three times the baseline. As depicted in Fig. 7, the greater the wind speed the more horizontal momentum the plume acquires. This momentum could cause the plume to travel closer the ground and elevate near-ground concentrations. Local hotspots appeared along the plume trajectory and also in the downwind canyon between building and uphill terrain.

4.5. Stack temperature

The effect of stack temperature was also investigated. The plume rise due to buoyancy is dependent on the stack temperature. For many boilers, stack economizers are often installed to recover waster heat from the hot exhaust gas and therefore improves boiler efficiency (DOE, 2010). It is estimated that the boiler efficiency can be increased by 1% by every 40° F reduction of exhaust temperature (DOE, 2012). Therefore, we varied the stack temperature by ±100 K from the baseline to investigate its impact on near-source environment. The resulting contour plot of $PM_{2.5}$ concentration was illustrated in Fig. 8. Raising the stack temperature could create more air buoyance and cause the plume to travel higher from the ground, and vice versa (Fig. 8). As a result, the near-ground concentration decreased with increasing stack temperature. In addition, $PM_{2.5}$ concentrations at the rooftop level remained more or less the same regardless the stack temperature, implying the dominant role of nearby building on stack plume dispersion.

4.6. Onsite vs. airport meteorological data

Dispersion modeling required in the permitting processes usually rely on meteorological data from the nearby airport. In our study, the nearest airport weather station (SYR) is about five miles

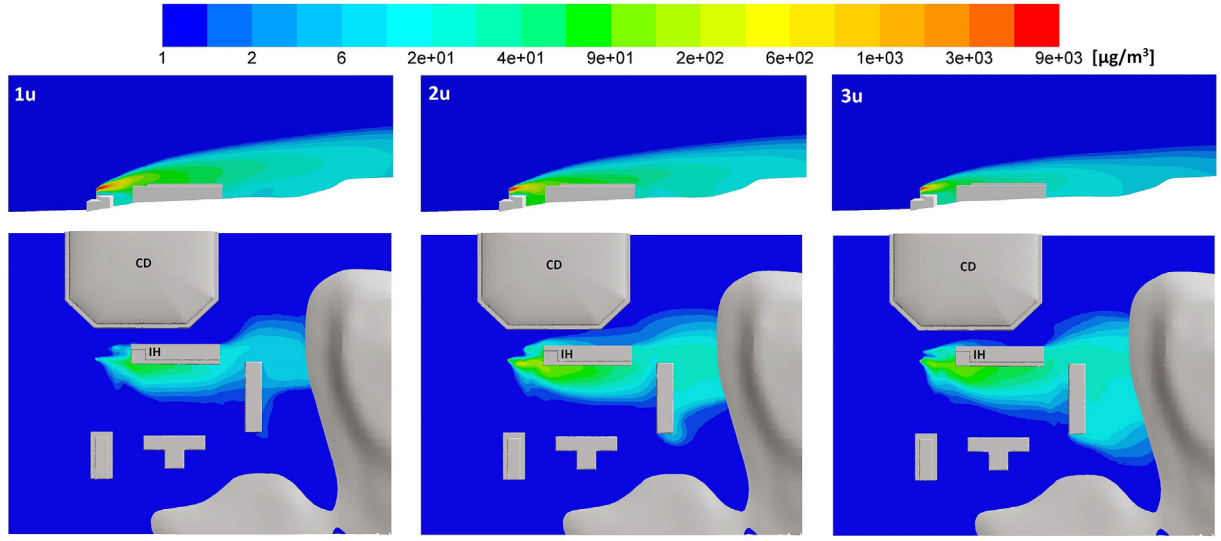

Fig. 7. Top view and side view of primary $PM_{2.5}$ concentration contour [μg m^{-3}] under three ambient wind speeds without ESP. *u* is the baseline wind speed at 2 m s^{-1}. The reference plane of the top view is taken at 1.5 m above the ground outside IH. Its location is displayed in the Supporting Information.

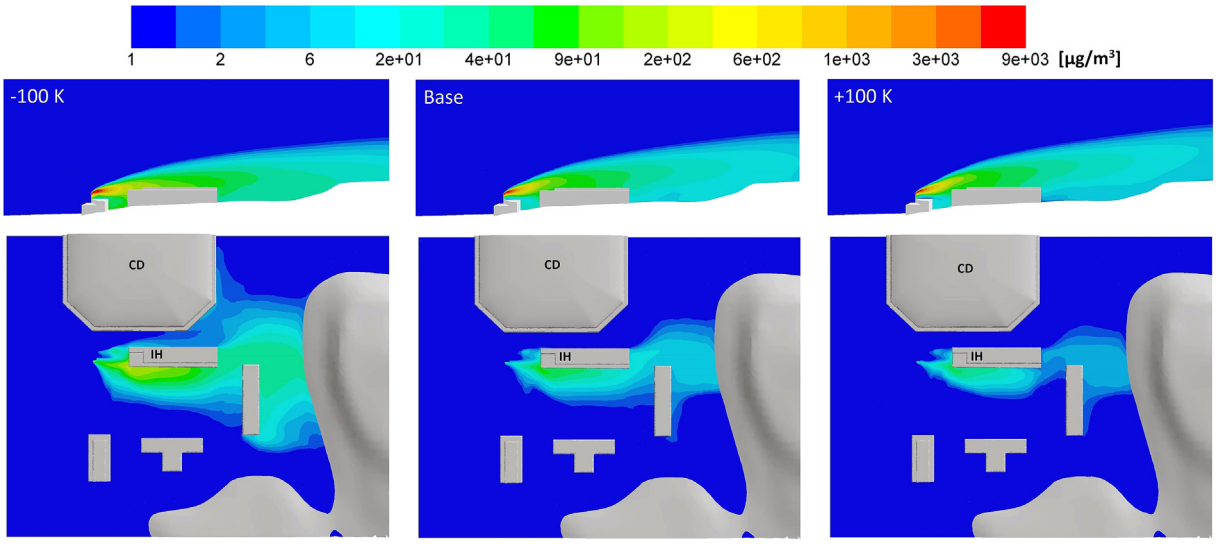

Fig. 8. Contour plot of the primary $PM_{2.5}$ concentrations [μg m^{-3}] at ±100 K of stack temperatures without ESP.

away from the boiler stack. We observed substantial discrepancies (Fig. S5 of the Supporting Information) by comparing the wind speed and directions measured at the upwind anemometer station with those from the airport. The difference likely resulted from hilly local terrain and major buildings near the site of interest. We simulated the plume dispersion based on wind data from both on-site and airport measurement at the same hour (11am on March 18th). Fig. S6 (Supporting Information) showed a comparison of the corresponding $PM_{2.5}$ concentration at a near-ground level. Although long-term simulation was not conducted in this study, the different plume trajectories demonstrated the importance of evaluating the suitability of airport weather data before performing any air quality modeling to avoid unintended error.

5. Conclusion

In this study, we investigated the spatial variations of $PM_{2.5}$ in a micro-environment near a commercial-scale biomass boiler. CFD-based Comprehensive Turbulent Aerosol Dynamics and Gas Chemistry (CTAG) model was employed to capture surrounding buildings and the hilly terrain. The selected biomass stack was uniquely located adjacent to two large buildings with rooftop access, which allowed us to detect the biomass plume under certain wind directions. Adequate agreement was obtained between predicted and onsite measurement in both flow fields and near-source primary $PM_{2.5}$ concentrations. Without ESP emission control, an almost seven times increase in primary $PM_{2.5}$ concentration was found in the surrounding environment under prevailing wind direction, the maximum ground-level concentration could exceed 35 μg m^{-3}, and the rooftop-level concentration could exceed 100 μg m^{-3}, posing a health risk to building occupants since particles can transport indoor through naturally ventilated windows and air handling units. In addition, higher wind speed could cause the plume to travel closer to the ground and elevate the near-ground concentration; raising the stack temperature could create more air buoyance and causes the plume to travel higher from the ground, and vice versa. Our study demonstrated the importance of installing emission control device for the biomass systems located in populous urban area as well as the need to take into account above-ground pollutant "hotspots".

Our analysis also identified notable discrepancies in near-source primary $PM_{2.5}$ concentrations between using on-site weather measurement and data from nearest airport weather station. These differences showed the importance of evaluating the suitability of weather data for neighborhood-scale air quality modeling. In the case where complex terrain and high-rise buildings are adjacent to the location of interest, on-site measurement is highly recommended to obtain reliable air quality simulations. Furthermore, we found that strategies that are often used to improve boiler efficiency, i.e., stack economizer, could elevate the near-ground primary$PM_{2.5}$ concentrations by reducing the plume rise. This is a tradeoff between near-source environment and boiler efficiency. Therefore, simply targeting on high energy efficiencies may deteriorate the air quality of surrounding environment as an unintended consequence.

Acknowledgement

The authors acknowledge the funding support from the New York State Energy Research and Development Authority (NYSERDA). The kindly assistance by Michael Kelleher, Brian Boothroyd and Christopher Maroney at SUNY Environmental Science and Forestry (ESF), Peter Sala at Syracuse University and Kui Wang at Clarkson University was instrumental to the study.

Appendix A. Supplementary data

Supplementary data related to this article can be found at http://dx.doi.org/10.1016/j.envpol.2016.11.025.

References

Allen, G.A., Miller, P.J., Rector, L.J., Brauer, M., Su, J.G., 2011. Characterization of valley winter woodsmoke concentrations in Northern NY using highly time-resolved measurements. Aerosol Air Qual. Research 11, 519–530.
Blocken, B., 2015. Computational fluid dynamics for urban physics: importance, scales, possibilities, limitations and ten tips and tricks towards accurate and reliable simulations. Build. Environ. 91, 219–245.
Boman, B.C., Forsberg, A.B., Järvholm, B.G., 2003. Adverse health effects from ambient air pollution in relation to residential wood combustion in modern society. Scand. J. Work, Environ. Health 29, 251–260.
Cebeci, T., Bradshaw, P., 1977. Momentum Transfer in Boundary Layers, vol. 407. Hemisphere Publishing Corp.; New York, McGraw-Hill Book Co., Washington, DC, p. 1977; 1.
Chandrasekaran, S.R., Laing, J.R., Holsen, T.M., Raja, S., Hopke, P.K., 2011. Emission characterization and efficiency measurements of high-efficiency wood boilers. Energy & Fuels 25, 5015–5021.

Cimorelli, A.J., Perry, S.G., Venkatram, A., Weil, J.C., Paine, R.J., Wilson, R.B., et al., 2005. AERMOD: a dispersion model for industrial source applications. Part I: general model formulation and boundary layer characterization. J. Appl. Meteorology 44, 682–693.
Demirbas, A., 2005. Potential applications of renewable energy sources, biomass combustion problems in boiler power systems and combustion related environmental issues. Prog. energy Combust. Sci. 31, 171–192.
DOE, 2010. Steam Generation Efficiency Module, Efficiency Definition Section.
DOE, 2012. Use Feedwater Economizers for Waster Heat Recovery.
Germano, M., Piomelli, U., Moin, P., Cabot, W.H., 1991. A dynamic subgrid-scale eddy viscosity model. Phys. Fluids A Fluid Dyn. (1989-1993) (3), 1760–1765.
Glasius, M., Ketzel, M., Wåhlin, P., Jensen, B., Mønster, J., Berkowicz, R., et al., 2006. Impact of wood combustion on particle levels in a residential area in Denmark. Atmos. Environ. 40, 7115–7124.
Gousseau, P., Blocken, B., Stathopoulos, T., van Heijst, G.J.F., 2011. CFD simulation of near-field pollutant dispersion on a high-resolution grid: a case study by LES and RANS for a building group in downtown Montreal. Atmos. Environ. 45, 428–438.
Hanna, S.R., 1993. Uncertainties in air quality model predictions. Boundary-Layer Meteorol. 62, 3–20.
Klein, M., 2005. An attempt to assess the quality of large eddy simulations in the context of implicit filtering. Flow, Turbul. Combust. 75, 131–147.
Kraichnan, R.H., 1970. Diffusion by a random velocity field. Phys. Fluids (1958-1988) (13), 22–31.
Larson, T.V., Koenig, J.Q., 1994. Wood smoke: emissions and noncancer respiratory effects. Annu. Rev. public health 15, 133–156.
Larson, T., Su, J., Baribeau, A.-M., Buzzelli, M., Setton, E., Brauer, M., 2007. A spatial model of urban winter woodsmoke concentrations. Environ. Sci. Technol. 41, 2429–2436.
Launder, B.E., Spalding, D.B., 1974. The numerical computation of turbulent flows. Comput. Methods Appl. Mech. Eng. 3 (2), 269–289.
Lind, T., Hokkinen, J., Jokiniemi, J.K., Saarikoski, S., Hillamo, R., 2003. Electrostatic precipitator collection efficiency and trace element emissions from Co-Combustion of biomass and recovered fuel in fluidized-bed combustion. Environ. Sci. Technol. 37, 2842–2846.
Mathey, F., Cokljat, D., Bertoglio, J.P., Sergent, E., 2006. Assessment of the vortex method for large eddy simulation inlet conditions. Prog. Comput. Fluid Dyn., Int. J. 6, 58–67.
Maykut, N.N., Lewtas, J., Kim, E., Larson, T.V., 2003. Source apportionment of PM2.5 at an urban improve site in seattle, Washington. Environ. Sci. Technol. 37, 5135–5142.
Moffat, R.J., 1988. Describing the uncertainties in experimental results. Exp. Therm. Fluid Sci. 1, 3–17.
Naeher, L.P., Brauer, M., Lipsett, M., Zelikoff, J.T., Simpson, C.D., Koenig, J.Q., et al., 2007. Woodsmoke health effects: a review. Inhal. Toxicol. 19, 67–106.
Petersen, R.L., Cochran, B.C., Carter, J.J., 2002. Specifying exhaust and intake systems. ASHRAE J. 44, 30–32.
Petrov, O., Bi, X., Lau, A., 2015. Impact assessment of biomass-based district heating systems in densely populated communities. Part I: dynamic intake fraction methodology. Atmos. Environ. 115, 70–78.
Pullen, J., Boris, J.P., Young, T., Patnaik, G., Iselin, J., 2005. A comparison of contaminant plume statistics from a Gaussian puff and urban CFD model for two large cities. Atmos. Environ. 39, 1049–1068.
Ries, F.J., Marshall, J.D., Brauer, M., 2009. Intake fraction of urban wood smoke. Environ. Sci. Technol. 43, 4701–4706.
Rodi, W., 1997. Comparison of LES and RANS calculations of the flow around bluff bodies. J. Wind Eng. Industrial Aerodynamics 69–71, 55–75.
RSG Inc, 2011. Combined Heat and Power Plant Permit Application for SUNY College of Environmental Science and Forestry.
Salim, S.M., Buccolieri, R., Chan, A., Di Sabatino, S., 2011. Numerical simulation of atmospheric pollutant dispersion in an urban street canyon: comparison between RANS and LES. J. Wind Eng. Industrial Aerodynamics 99, 103–113.
Schauer, J.J., Rogge, W.F., Hildemann, L.M., Mazurek, M.A., Cass, G.R., Simoneit, B.R.T., 1996. Source apportionment of airborne particulate matter using organic compounds as tracers. Atmos. Environ. 30, 3837–3855.
Sini, J.-F., Anquetin, S., Mestayer, P.G., 1996. Pollutant dispersion and thermal effects in urban street canyons. Atmos. Environ. 30, 2659–2677.
Stedman, D.H., 1989. Automobile carbon monoxide emission. Environ. Sci. Technol. 23, 147–149.
Steffens, J.T., Heist, D.K., Perry, S.G., Zhang, K.M., 2013. Modeling the effects of a solid barrier on pollutant dispersion under various atmospheric stability conditions. Atmos. Environ 69, 76–85.
Steffens, J.T., Heist, D.K., Perry, S.G., Isakov, V., Baldauf, R.W., Zhang, K.M., 2014. Effects of roadway configurations on near-road air quality and the implications on roadway designs. Atmos. Environ 94, 74–85.
Su, J.G., Buzzelli, M., Brauer, M., Gould, T., Larson, T.V., 2008. Modeling spatial variability of airborne levoglucosan in Seattle, Washington. Atmos. Environ. 42, 5519–5525.
Su, J.G., Hopke, P.K., Tian, Y., Baldwin, N., Thurston, S.W., Evans, K., et al., 2015. Modeling particulate matter concentrations measured through mobile monitoring in a deletion/substitution/addition approach. Atmos. Environ. 122, 477–483.
Tominaga, Y., Stathopoulos, T., 2011. CFD modeling of pollution dispersion in a street canyon: comparison between LES and RANS. J. Wind Eng. Industrial Aerodynamics 99, 340–348.
Tong, Z., Zhang, K.M., 2015. The near-source impacts of diesel backup generators in urban environments. Atmos. Environ. 109, 262–271.
Tong, Z., Wang, Y.J., Patel, M., Kinney, P., Chrillrud, S., Zhang, K.M., 2012. Modeling spatial variations of black carbon particles in an urban highway-building environment. Environ. Sci. Technol. 46, 312–319.
Tong, Z., Baldauf, R.W., Isakov, V., Deshmukh, P., Max Zhang, K., 2016. Roadside vegetation barrier designs to mitigate near-road air pollution impacts. Sci. Total Environ. 541, 920–927.
Tseng, Y.-H., Meneveau, C., Parlange, M.B., 2006. Modeling flow around bluff bodies and predicting urban dispersion using large eddy simulation. Environ. Sci. Technol. 40, 2653–2662.
USEPA, 2004. User's Guide for the AERMOD Meteorological Preprocessor (AERMET). U.S. Environmental Protection Agency.
Wang, Y.J., Zhang, K.M., 2012. Coupled turbulence and aerosol dynamics modeling of vehicle exhaust plumes using the CTAG model. Atmos. Environ 59, 284–293.
Wang, X., Westerdahl, D., Chen, L.C., Wu, Y., Hao, J., Pan, X., et al., 2009. Evaluating the air quality impacts of the 2008 Beijing Olympic games: on-road emission factors and black carbon profiles. Atmos. Environ. 43, 4535–4543.
Wang, Y., Hopke, P.K., Rattigan, O.V., Xia, X., Chalupa, D.C., Utell, M.J., 2011a. Characterization of residential wood combustion particles using the two-wavelength aethalometer. Environ. Sci. Technol. 45, 7387–7393.
Wang, Y.J., DenBleyker, A., McDonald-Buller, E., Allen, D., Zhang, K.M., 2011b. Modeling the chemical evolution of nitrogen oxides near roadways. Atmos. Environ. 45, 43–52.
Wang, X., Westerdahl, D., Hu, J., Wu, Y., Yin, H., Pan, X., et al., 2012. On-road diesel vehicle emission factors for nitrogen oxides and black carbon in two Chinese cities. Atmos. Environ. 46, 45–55.
Wang, Y.J., Nguyen, M.T., Steffens, J.T., Tong, Z., Wang, Y., Hopke, P.K., et al., 2013a. Modeling multi-scale aerosol dynamics and micro-environmental air quality near a large highway intersection using the CTAG model. Sci. Total Environ. 443, 375–386.
Wang, Y.J., Yang, B., Lipsky, E.M., Robinson, A.L., Zhang, K.M., 2013b. Analyses of turbulent flow fields and aerosol dynamics of diesel engine exhaust inside two dilution sampling tunnels using the CTAG model. Environ. Sci. Technol. 47, 889–898.
Wang, K., Hopke, P.K., Thimmaiah, D., 2015. Emission Characterization of a Large Scale Wood Pellet Combined Heat and Power System. American Association for Aerosol Research 34th Annual Conference.
Westerdahl, D., Wang, X., Pan, X., Zhang, K.M., 2009. Characterization of on-road vehicle emission factors and microenvironmental air quality in Beijing, China. Atmos. Environ. 43, 697–705.
Wood, C.R., Jarvl, L., 2012. Urban climate observations in Helsinki. Magzine Finn. Air Pollut. Soc. (3), 3.
Xie, Z., Castro, I., 2006. LES and RANS for turbulent flow over arrays of wall-mounted obstacles. Flow, Turbul. Combust. 76, 291–312.
Zheng, M., Cass, G.R., Schauer, J.J., Edgerton, E.S., 2002. Source apportionment of PM2.5 in the southeastern United States using solvent-extractable organic compounds as tracers. Environ. Sci. Technol. 36, 2361–2371.